A Detailed Kinetico-Mechanistic Investigation on the Palladium C–H Bond Activation in Azobenzenes and their Monopalladated Derivatives

Alen Bjelopetrović,[a‡] Dajana Barišić,[a‡] Zrinka Duvnjak,[b] Ivan Džajić,[b] Marina Juribašić Kulcsár,[a] Ivan Halasz,[a] Manuel Martínez,[c,d*] Ana Budimir,[b*] Darko Babić,[a*] and Manda Ćurić,[a*]

[a]Ruđer Bošković Institute, Division of Physical Chemistry, Bijenička 54, HR-10000 Zagreb, Croatia

[b]University of Zagreb, Faculty of Pharmacy and Biochemistry, Ante Kovačića 1, 10000 Zagreb, Croatia

[c]Departament de Química Inorgànica i Orgànica, Secció de Química Inorgànica, Martí i Franquès 1-11, E-08028 Barcelona, Spain

[d]Institute of Nanoscience and Nanotechnology (IN2UB), Universitat de Barcelona, Barcelona, Spain

Supporting Information Placeholder

ABSTRACT: Palladium C–H bond activation in azobenzenes with R_1 and R_2 at *para*-positions of the phenyl rings (R_1=NMe_2, R_2=H (**L1**); R_1=NMe_2, R_2=Cl (**L2**); R_1=NMe_2, R_2=I (**L3**); R_1=NMe_2, R_2=NO_2 (**L4**); R_1=H, R_2=H (**L5**)) and their monopalladated derivatives, using *cis*-[$PdCl_2(DMF)_2$], has been studied in detail by *in situ* ^{1}H NMR spectroscopy in *N*,*N*-dimethylformamide-d_7 (DMF-d_7) at room temperature; the same processes have been monitored in parallel via time-resolved UV-Vis spectroscopy in DMF at different temperatures and pressures. The final goal was to achieve, from a kinetico-mechanistic perspective, a complete insight on previously reported reactivity results. The results suggest the operation of an electrophilic concerted metallation and deprotonation mechanism for both the mono- and dipalladation reactions, occurring from the coordination compound and the monopalladated intermediates, respectively. The process involves deprotonation of the C–H bond assisted by the presence of a coordinated DMF molecule, that acts as a base. For the first time, NMR monitoring provides a direct evidence of all the intermediate stages, that is: *i*) coordination of the azo ligand to Pd^{II} center, *ii*) formation of the monopalladated species, *iii*) coordination of the monopalladated species to another Pd^{II} unit, which finally result in the *iv*) formation of the dipalladated product. All of these species have been identified as intermediates in the dipalladation of azobenzenes, evidenced also by UV-Vis spectroscopy time-resolved monitoring. The data also confirms that the cyclopalladation of asymmetrically substituted azobenzenes occurs by two concurrent reaction paths. In order to identify the species observed by NMR and by UV-Vis spectroscopies, the final products, intermediates and the Pd^{II} precursor have been prepared and characterized by X-ray diffraction, IR and NMR spectroscopies. DFT calculations have also been used in order to explain the isomerism observed for the isolated complexes, as well to assign their NMR and IR spectra.

INTRODUCTION

Cyclopalladation continuously attracts considerable interest, not only as the most direct route for the synthesis of palladacycles,[1] but also as a generally important reaction in organic synthetic chemistry.[2] Palladacycles are identified as crucial intermediates in many organic reactions promoted by palladium precursors, that result in functionalized hydrocarbons.[1,2] Therefore, a detailed understanding of cyclopalladation pathways of different organic substrates is essential. Cyclopalladation is recognized as a two-step reaction involving the coordination of palladium center by a directing group, which leads to selective intramolecular activation of the C–H bond, resulting in the formation of the Pd–C bond with simultaneous proton release and ring closure.[1c,3] This mechanism is supported by our kinetico-mechanistic studies on a variety of compounds,[4] and specifically by our previous studies of the mono- and dicyclopalladation of azobenzene and its 4,4'-functionalized derivatives using *trans*-[$PdCl_2(MeCN)_2$] as the precursor.[4b]

The kinetics of the latter processes had been studied by UV-Vis time-resolved spectroscopy in *N*,*N*-dimethylformamide (DMF) at room temperature, as this is the solvent for numerous Pd^{II}-catalyzed reactions.[2f,5] Rationalization of the experimental kinetic data by DFT calculations had provided a convincing mechanistic picture of the electrophilic attack at the phenyl ring within the Pd-azobenzene complex.[4a,b]

To provide a complete understanding of that work, here we present a kinetico-mechanistic study of the cyclopalladation of azobenzenes and their monopalladated compounds (Chart 1) both by NMR and UV-Vis spectroscopies. The time-resolved ^{1}H NMR study has allowed, for the first time, a full and detailed insight into the nature and reactivity of the intermediates formed during these reactions. The Pd^{II} precursor, *cis*-[$PdCl_2(DMF)_2$], and most of the detected intermediates have been isolated and characterized both structurally and spectroscopically. These results provided direct evidence that dipalladation of azobenzenes proceeds via two parallel

pathways when asymmetrically substituted azobenzenes are used, and that each of them consists of four consecutive steps. Furthermore, the UV-Vis spectroscopy at different temperatures and pressures has allowed for the first time the obtention of detailed kinetico-mechanistic information by determining activation parameters, both thermal ($\Delta H^{\ddagger}$, $\Delta S^{\ddagger}$) and pressure ($\Delta V^{\ddagger}$).

Chart 1. Molecular structure of the azobenzene and its coordination, mono- and dicyclopalladated derivatives, used in this study. Only α-isomers of An, Mn and MAn are shown.

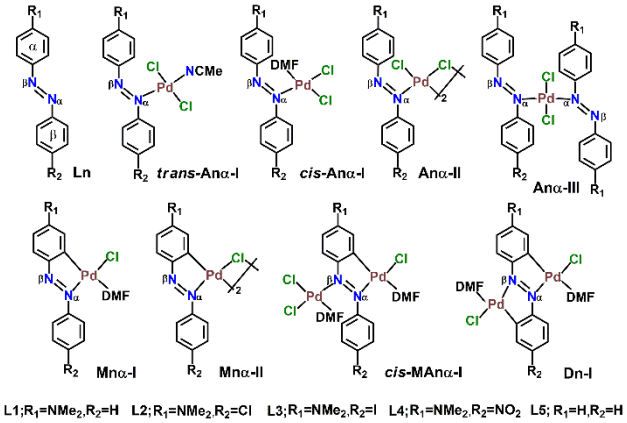

RESULTS AND DISCUSSION

Compounds. The Pd^{II} precursor, coordination, mono- and dipalladated complexes of the azobenzenes studied (Chart 1) have been isolated and structurally characterized by X-ray diffraction and IR spectroscopy in the solid-state, and by NMR spectroscopy in solution.

Pd^{II} precursor. *cis*-[$PdCl_2(DMF)_2$] was obtained in high yield by aging $PdCl_2$ in a vapor of *N*,*N*–dimethylformamide (DMF),[6] and also by evaporation and cooling of a DMF solution of $PdCl_2$. Its molecular structure, resolved by powder X-ray diffraction (PXRD), indicates a *cis*-configuration at the Pd^{II} center and the coordination of the oxygen donors from the two DMF ligands (Figure 1). The IR spectrum of the isolated product provided additional support for the *cis* configuration, as two bands are observed for both Pd–Cl and Pd–O stretching vibrations (Figure S2).

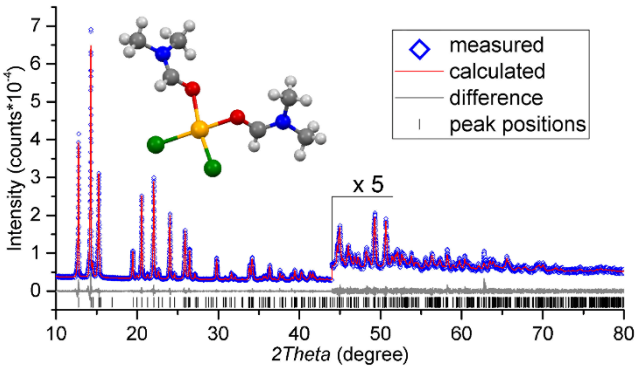

Figure 1. Powder X-ray diffraction of the calculated molecular structure of *cis*-[$PdCl_2(DMF)_2$] and its final Rietveld refinement.

Despite existing reports on the isolation and characterization of the *trans*-isomer,[7] all our attempts to obtain *trans*-[$PdCl_2(DMF)_2$] from DMF solutions were unsuccessful. Cooling down of the concentrated DMF solution of *cis*-[$PdCl_2(DMF)_2$] to -25°C resulted in quantitative precipitation only of the *cis*-isomer as confirmed by PXRD and IR spectra (Figures S1 and S2). DFT calculations support this finding, although only by a 1 kcal/mol free energy difference in favor of the *cis*-[$PdCl_2(DMF)_2$] isomer.[4b]

Coordination (acetonitrile derivatives *trans*-**Anα-I**, **Anα-II**, **Anα-III) and monopalladated (**DMF derivatives **Mnα-I**, **Mnα-II) compounds**. The coordination and monopalladated complexes were prepared in MeCN and DMF solution, respectively, by the procedure already developed for **A2α-I** and **M2α-I**.[8]

The reactions of **L1** and **L3** with $PdCl_2$ in a 1:1 molar ratio afforded the respective acetonitrile derivatives of *trans*-**A1α-I** and *trans*-**A3α-I** complexes, as confirmed by X-ray single-crystal diffraction analysis (Figures 3, S5 and S6) and NMR spectroscopy. Despite the fact that two isomers, α and β, can be formed in the reactions of $PdCl_2$ with the unsymmetrically substituted azobenzenes,[9] all the coordination compounds obtained show the palladium center bound to the N_α of azobenzene. Chart 1 shows the *cis*-**Anα-I** complexes with DMF, as they are the primary product of the reaction with *cis*-[$PdCl_2(DMF)_2$], and also the productive isomers in cyclopalladation;[4a] for this reason from now on in this work they weiil be reffered simply as **Anα-I**.

For **A1α**, **A2α** and **A3α** structures only monomeric species have been isolated, but for **A4α** a mixture of monomeric and dimeric coordination compounds **A4α-I** and **A4α-II** was obtained. Reaction of **L5** with $PdCl_2$ yielded exclusively the already known[10] *bis*-complex **A5-III**, regardless of the **L5** to Pd molar ratio used. The product was structurally identified by comparison of its powder diffraction (PXRD) pattern with that simulated from its known single crystal structure (Figure S3).[10]

Stirring in DMF solution the coordination complexes indicated above produces the monopalladated monomeric **M1α-I** and **M3α-I**, or dimeric **M4α-II** compounds. The analogous reaction with **A5-III** resulted in a mixture of free azobenzene ligand, monopalladated and dipalladated species. Neat **M5-II**, was only obtained by the reaction of **L5** with $Na_2[PdCl_4]$ in methanol, as already described.[11] The ^{1}H NMR spectral data, along with the elemental analysis (see Experimental), support the formulation of the isolated monopalladated products as monomeric [PdCl(**Ln**−H)(DMF)] (**M1α-I** and **M3α-I**) and dimeric $[Pd(\mu\text{-}Cl)(\mathbf{Ln}-H)]_2$ (**M4α-II** and **M5-II**) species. The molecular structure of the new monomeric **M1α-I** product, resolved by X-ray single-crystal diffraction, confirmed the formation of the isomer with the palladium center bonded to the N_α donor and to the phenyl ring bearing the electron-donating NMe_2 group (Figures 2, S7 and Table S1). The formation of the dimeric monopalladated azobenzene **M5-II** was confirmed by its powder diffraction (PXRD) pattern, which is in good agreement with that simulated from the already known single crystal structure[12] (Figure S4). ^{1}H NMR spectra of the dimeric **M4α-II** and **M5-II** compounds indicate that these convert into the monomeric **M4α-I** and **M5-I** species in DMF solution, with the shift pattern of their signals being equivalent to those of the **M1α-I – M3α-I** compounds.

Dipalladated azobenzenes (**Dn-I**). **D1-I – D5-I** were prepared in DMF by the reaction of **M1α-I**, **M2α-I**, **M3α-I**, **M4α-II** and **M5-II** with *cis*-$[PdCl_2(DMF)_2]$, which is a new procedure diverse from previous preparations that started directly from the azoderivatives **L1 - L5**.[4b]

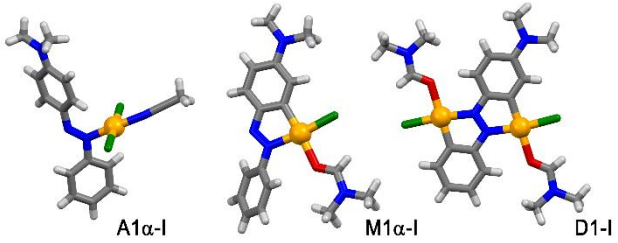

Figure 2. Molecular structures of *trans*-**A1α-**, **M1α-I** and **D1-I**.

The products were structurally identified by comparison with the PXRD, IR and NMR spectra of the already known compounds. Additionally, single crystals were obtained and analyzed for **D1-I** (Figures 2, S8 and Table S1); bond distances and angles around the palladium coordination sphere are similar to those found and calculated for other dipalladated azobenzenes.[4b,13]

DFT calculations on the speciation of the compounds studied. The different forms of the isolated coordination and monopalladated complexes prompted us to examine whether this isomerism can be attributed to diverse isomer stabilities. The equilibrium constants between **Anα-I**, **Anα-II** and **Anα-III** (in MeCN, from which they were isolated), as well as between **Mnα-I** and **Mnα-II** (in DMF, the solvent used in their preparation), were evaluated from the quantum-chemical free energies of the corresponding molecular species. The calculated equilibrium compositions involved only **Anα-I** and **Anα-III** species, with negligible concentrations of **Anα-II** complexes. **A1α-I** and **A5-III** were predicted as major forms in agreement with experimental findings. The calculations indicated **A2α-III** and **A3α-III** as dominant isomeric species, in contrast to the fact that only **A2α-I** and **A3α-I** have been isolated. Similarly, **A4α-III** was predicted as dominant, in opposition to the experimentally obtained mixture of **A4α-I** and **A4α-II**. All monopalladated monomeric species, **Mnα-I**, were predicted as dominant, contrary to the experimentally observed **M4α-II**. The disagreements can be assigned to the unaccounted solvent interactions or crystal packing effects (different solubilities). But it is also possible that the presently available computational methods are not sufficiently precise to predict fine differences in the isomer stabilities. Agreement with the experimental findings can be established by shifting of the computational results within 1 kcal/mol, which is commonly considered as a computational error margin.

Kinetico-mechanistic studies. Our previous UV-Vis time-resolved monitoring of the reactions at 25 °C and atmospheric pressure had indicated that the dipalladation of the azobenzenes used in this study is a multistep process. The full reactivity involves the formation of the intermediates **Anα-I** and **MAnα-I** (see Chart 1) in fast pre-equilibria, prior to the rate-determining steps generating mono- and dipalladated species **Mnα-I** and **Dn-I**, respectively, (Scheme 1 and equations (1) and (2)).[4b]

UV-Vis time-resolved monitoring. Since the full set of activation parameters, $\Delta H^{\ddagger}$, $\Delta S^{\ddagger}$ and $\Delta V^{\ddagger}$, provide determinant information on the cyclopalladation mechanism,[4e,15] the reactions of **L1-L4** and **M1α-I – M4α-I**, with *cis*-$[PdCl_2(DMF)_2]$ in DMF were monitored by UV-Vis time-resolved spectroscopy at varying temperatures and pressures.

Scheme 1. Full dipalladation process of the azobenzenes studied.[4b] {Pd} represents *cis*-$[PdCl_2(DMF)_2]$.

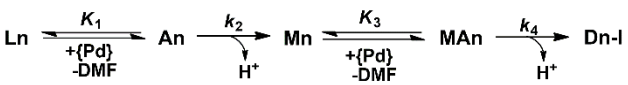

$$k_{obs(1)} = \frac{k_2 K_1 [\mathrm{Pd}]}{1 + K_1 [\mathrm{Pd}]} \qquad (1)$$

$$k_{obs(2)} = \frac{k_4 K_3 [\mathrm{Pd}]}{1 + K_3 [\mathrm{Pd}]} \qquad (2)$$

All reactions were carried out under pseudo-first order conditions, with a large molar excess of *cis*-[$PdCl_2(DMF)_2$]. Monitoring of the reactions of **L1**-**L4** with *cis*-[$PdCl_2(DMF)_2$] indicated the presence of a two-step sequence in the full palladation process, as observed before.[4b]

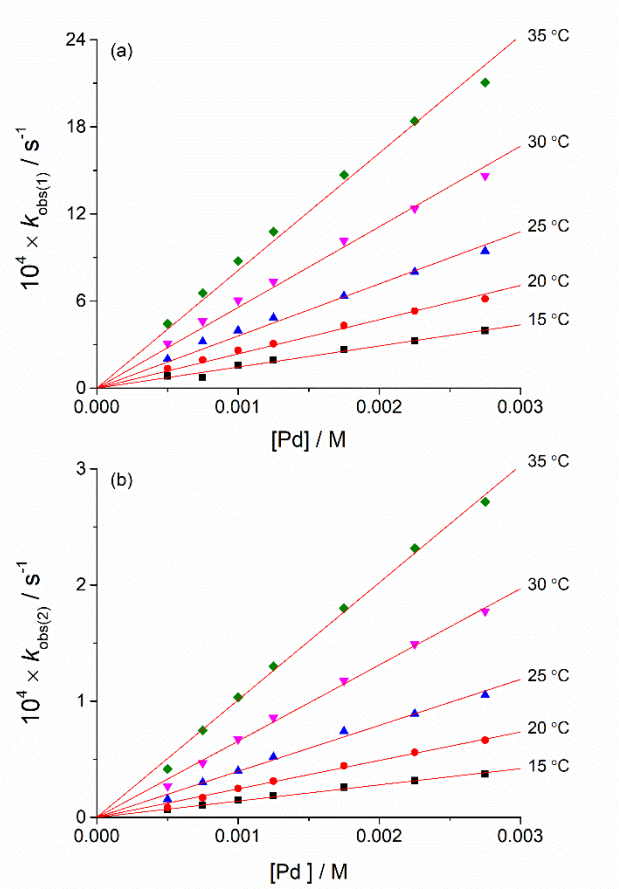

Figure 3. Dependence of the pseudo-first-order rate constants for the first, $k_{obs(1)}$, (a) and second, $k_{obs(2)}$, (b) cyclopalladation of **L2** on [Pd] in DMF at different temperatures; [**L2**] = 25 μM.

The observed pseudo-first order constants $k_{obs(1)}$ and $k_{obs(2)}$ were calculated from the time-resolved spectral changes using a consecutive A → B → C model. The dependence of $k_{obs(1)}$ and $k_{obs(2)}$ on the *cis*-[$PdCl_2(DMF)_2$] concentration (in excess, Figure 3), lead us to consider as valid the reaction mechanism and the rate law depicted by Scheme 1 and equations (1) and (2) for the systems studied. The lack of curvature in the plots of Figure 3 indicate that K_1 and K_3 have sufficiently low values to avoid a saturation behaviour.[15] The values of the k_2K_1 and k_4K_3 products for the reactions of the **L1**-**L4** ligands, determined from the slopes of the $k_{obs(1)}$ and $k_{obs(2)}$ *versus* [Pd] data at variable temperature and pressure (Table S2, Figures 3 and S9), agree with former experiments at room temperature.[4b]

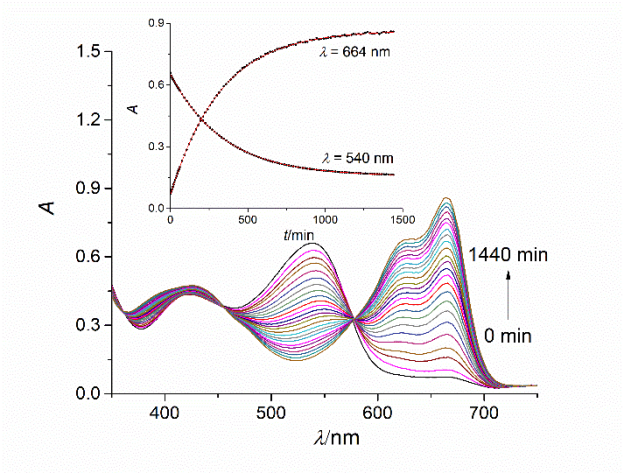

Figure 4. UV-Vis time-resolved spectral changes for the reaction *cis*-[$PdCl_2(DMF)_2$] + **M2α-I** → **D2-I**, in DMF. **[M2α]** = 25 μM, **[**Pd] = 1.0 mM, T = 25 °C. The inset shows the kinetic traces at 540 and 664 nm, along with their fitting to an A → B process.

As shown in Figure 4, the time-resolved spectral changes recorded during the reaction of *cis*-[$PdCl_2(DMF)_2$] with **M1α-I** – **M4α-I** can be fitted to the simple A → B model. The pseudo-first-order rate constants k_{obs} derived show a linear dependence on the palladium concentration (Figure S10), and produce a set of second order rate constants, k_4K_3, (Table S2), that are expected to be equivalent to that obtained for the second part of the mechanism in Scheme 1, i.e., the second cyclopalladation of **Ln**.[4b]

The fitting of the variation of k_2K_1 and k_4K_3 for the reactions of **Ln**, or k_4K_3 for those of **Mnα-I**, at different temperatures, using the standard Eyring plots (Figures 5a and S11), produce the values of the thermal activation parameters ($\Delta H^{\ddagger}$ and $\Delta S^{\ddagger}$) indicated in Table 1.

The pressure activation parameters ($\Delta V^{\ddagger}$), determined by the variation of the second order rate constants for the reaction of **Ln** (calculated as k_{obs}/[Pd], see Experimental) at different pressures, using the standard ln(k) versus P equation (Figures 5b and S12), are also summarized in Table 1. The pressure variation of the values of k_4K_3 for the reaction to **Dn-I** from the **Mnα-I** intermediates instead of the **Ln**, was also conducted at varying pressures. As seen in Figures 5b and S12 and Table 1, the values determined are in very close agreement with those obtained for the second step observed on the reaction of the precursor with of **Ln**. Consequently, $\Delta V_2^{\ddagger}$ was considered independent of the origin of the monometallated intermediate within the error involved in its determination

Table 1. Summary of the kinetic (298 K) and thermal and pressure activation parameters determined for the cyclopalladation reaction of azobenzenes L1-L4 and their monopalladated derivatives M1α-I - M4α-I in DMF solution.

Compound	$^{298}k_2K_1$ M^{-1} s^{-1}	$\Delta H_1^{\ddagger}$ kJ mol^{-1}	$\Delta S_1^{\ddagger}$ JK^{-1} mol^{-1}	$\Delta V_1^{\ddagger}$ cm^3 mol^{-1}	$^{298}k_4K_3$ M^{-1} s^{-1}	$\Delta H_2^{\ddagger}$ kJ mol^{-1}	$\Delta S_2^{\ddagger}$ J K^{-1} mol^{-1}	$\Delta V_2^{\ddagger}$ cm^3 mol^{-1}
L1	0.44	64 ± 2	–37 ± 6	–12 ± 1	0.060	60 ± 3	–67 ± 8	–15 ± 2
M1α-I	–	–	–	–	0.071	59 ± 1	–71 ± 2	–11 ± 2
L2	[a]0.39	62 ± 2	–47 ± 6	–11 ± 2	[a]0.040	70 ± 1	–36 ± 3	–8± 1
M2α-I	–	–	–	–	0.046	63 ± 2	–60 ± 6	–9± 1
L3	0.40	57 ± 2	–62 ± 7	–11 ± 2	0.055	64 ± 1	–52 ± 3	–12 ± 2
M3α-I					0.067	62 ± 1	–59 ± 3	–11 ± 1
L4	0.25	63 ± 1	–47 ± 3	–8.3 ± 0.1	0.030	66 ± 3	–50 ± 8	–8 ± 1
M4α-I	–	–	–	–	0.038	64 ± 1	–62 ± 4	–7 ± 1

[a]The different values from reference[4b] are due to a purification of the commercial **L2** ligand done in this work.

The interpretation of the values of the activation parameters summarized in Table 1, is not straightforward in several ways. To start with, the values cannot be assigned to a simple kinetic step, as the determined rate constants are composites of an equilibrium constant for the formation of intermediates **Anα-I** or **MAnα-I** and the first-order rate constant for the subsequent C–H bond activation (Scheme 1 and equations 1 and 2). Therefore, the thermal and the pressure activation parameters correspond to this product, and include the values of ΔH^o, ΔS^o, and ΔV^o for the formation equilibrium constants (K_1 and K_3). Even more, only the values corresponding to the palladation from **Mnα-I** correspond to a proper single reaction pathway. For all the other processes studied, the reactivity corresponds to that of a mixture of the α and the putative β isomer of **An-I** and **Mn-I** complexes (see the next section and Scheme 2). This is evident from the values of $\Delta H_2^{\ddagger}$ and $\Delta S_2^{\ddagger}$ collected in Table 1 for the dipalladation of the **Ln** derivatives, that correspond to the average of the reaction occurring on the α and β isomers of **Mn-I**.

Interestingly, comparison of the data observed for the second palladation processes indicates that the values expected for the reactions occurring on the α unit of the **Mnβ-I** compounds should have larger activation enthalpies and less negative activation entropies, in order to attain the average data obtained as the second palladation of **Ln**. It seems clear that the metalation of the β-monometalated complexes, **MAnβ-I**, by the palladium attached to $N_α$, has an earlier transition state with lower ordering but with higher enthalpy

demands that has to be related to the presence of the donor –NMe_2 on the *meta* position of the activating C–H bond. This conclusion is further supported by the Wiberg bond orders of the Pd–C and C–H bonds in the transition states of **MAn-I → Dn-I** transformations (Table S13 and Figure S34 in SI_2). The Pd–C bond orders in **MAnβ-I → Dn-I** transition states are lower than in the **MAnα-I → Dn-I** counterparts, and the opposite relation holds for the C–H bond orders (see also the last paragraph in this section).

Even with these difficulties in their final interpretation, plus the fact that the DMF-assisted process involves the exit of a positively charged $\{HDMF\}^+$ unit, the values of the activation parameters depicted in Table 1 are within the range of those determined for other base-assisted C–H bond activations.[3a-3c,4d] The negative values of $\Delta S^{\ddagger}$ and $\Delta V^{\ddagger}$ for both palladation steps agree with the presence of a highly ordered transition state in the rate determining step, which is supported by computational studies of the cyclopalladation mechanism.[3a,-3c,4a,b,d] In this respect, the values determined for $\Delta S^{\ddagger}$ lay even lower than the lower-end of the available data for reactions having AcO^- or AcOH as coordinating base-assisting ligands.[3a] This observation is in line with the fact that the less coordinating (AcO^- < AcOH < DMF) assisting base produces a lower degree of ordering on going to the transition state, that is occurs at a later position of the reaction coordinate.

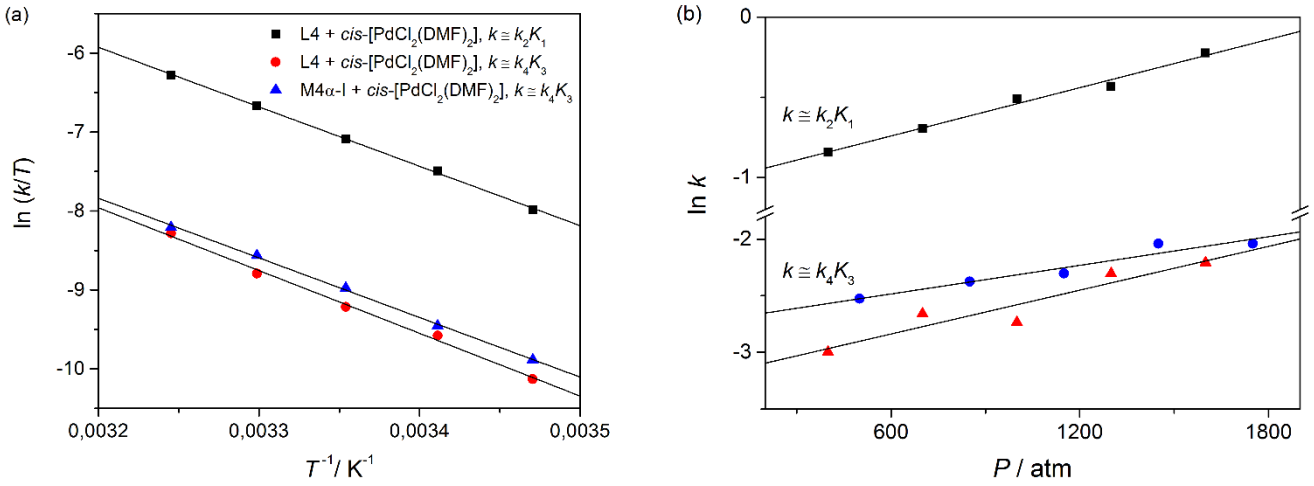

Figure 5. a) Eyring plots for the reaction sequence **L4** + *cis*-$[PdCl_2(DMF)_2]$ → **M4α–I** + *cis*-$[PdCl_2(DMF)_2]$ → **D4-I** (k_2K_1 and k_4K_3), and the reaction **M4α–I** + *cis*-$[PdCl_2(DMF)_2]$ → **D4-I** (k_4K_3). b) ln *k* versus *P* plot for the reaction sequence **L1** + *cis*-$[PdCl_2(DMF)_2]$ → **M1α–I** + *cis*-$[PdCl_2(DMF)_2]$ → **D1-I** (k_2K_1 and k_4K_3, red triangle) and the reaction **M1α–I** + *cis*-$[PdCl_2(DMF)_2]$ → **D1-I** (k_4K_3, blue circles).

While all these findings fit well into the concerted metallation and deprotonation (CMD) mechanism proposed earlier,[3b,c,4d] some recent results[2c,16a] indicate that this mechanism in fact comprises two subclasses distinguished by the site selectivity preferences. Those with nucleophilic affinity, towards more acidic C-H bonds, are termed *standard* CMD,[16] while those with electrophilic character are denoted as *electrophilic* CMD (*e*CMD). A clear identifying characteristics of this diversity is the Wiberg bond orders of the Pd–C and C–H bonds directly involved in the C–H activation.[2c,16a] A sum of these two Wiberg bond orders in the transition state geometry was established as a representative quantity. A critical value of 0.8 distinguishes the transition states of the standard CMD mechanism (with sum <0.8), from those in the *e*CMD class (sum >0.8). In the present study, from the calculated transition state geometries[4b] for all the ligands, for both cyclopalladation steps, and α,β-paths, the sum of the two Wiberg indices are well above 0.8 (0.90-0.93, for all but **MA5-I → D5** which has slightly outlying value of 0.85, Table S13 and Figure 34 in SI-2), thus indicating an *e*CMD mechanism. The electrophilic nature of the present mechanism, as proven by the preference for C–H bonds at the more electron-rich aromatic rings, also agrees with the *meta*-properties of the *e*CMD mechanism.

NMR time-resolved monitoring. Since the coordination intermediates cannot be detected by UV-Vis spectroscopy, time-resolved ^{1}H NMR monitoring of the reactions of **Ln** and **Mnα-I** with *cis*-$[PdCl_2(DMF)_2]$ was conducted (Figures S13-S24). The procedure enabled the obtention of the concentration profiles of the species indicated in Scheme 2 (Figures S25-S33) and provided a detailed insight into the reaction dynamics.

Scheme 2. Kinetic model for the dipalladation of the azobenzenes used with cis-$[PdCl_2(DMF)_2]$ precursor (labeled as {Pd}).

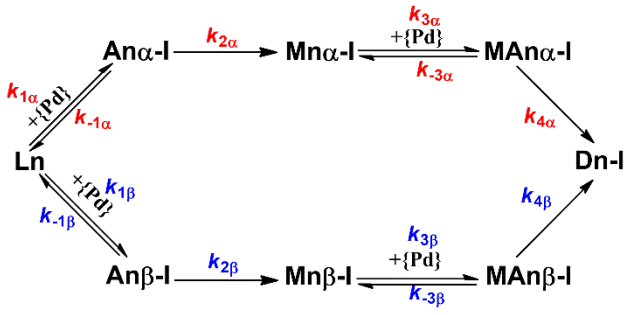

The kinetic model in Scheme 2 assumes two parallel cyclopalladation reaction pathways. These occur on the two possible isomers of the initial coordination compounds, that is **Anα-I** and **Anβ-I**. In both pathways, and for both mono- and di-cyclopalladation steps, the formation of each coordination complex is assumed to be a reversible process, while the subsequent proton transfer is considered as rate determining and irreversible, due to the removal of the aromatic proton. The ^{1}H NMR spectra of the reaction mixture at different times are consistent with the presence of the species indicated in Scheme 2. The signals of the **Anα-I** species were easily identified from the known spectra of the isolated α-adducts, and those of **Anβ-I** were recognized by their similarity with the α-counterparts (Figures S13-S16).

Confirmation of the formation of both α- and β-isomers was obtained from the reaction of **L5** with *cis*-[PdCl$_2$(DMF)$_2$], where a single set of signals for **A5-I** was observed, given the equivalence of N$_\alpha$ and N$_\beta$ in **L5** (Figures S17-S19). The signals of the **Mnβ-I** complexes were assigned based on similarities of their dynamics and NMR shifts with **Mnα-I** species, and those of **MAnα,** were ascertained from the simpler reactions initiated from **Mnα-I** (Figures S21-24). The concentrations of **MAnβ** were found, in all cases, too low to be detected or quantified reliably from the NMR spectra.

As indicated in the Experimental section, the NMR time-resolved speciation data was fed into the Dynafit software,[17] with the kinetic model corresponding to Scheme 2. Even though **M4α-I** and **M5-I** were effectively isolated as **M4α-II** and **M5-II**, the formation of the final **Dn-I** complexes always proceeded via **Mnα-I**. Also, although azobenzenes are potentially able to bind to two Pd centers, these species were never detected despite the 10-fold excess of Pd precursor used in the experiments. In this respect, the computational results do not provide any reason for such an absence,[4b] hence their presence as transient species cannot be ruled out. However, if present in any significant amounts, the species should manifest themselves in the reaction kinetics, a fact that has not been observed.

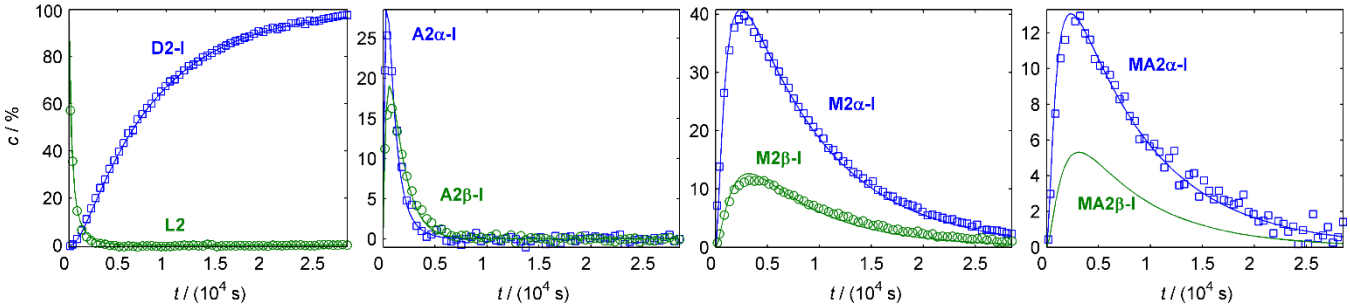

Figure 6. Experimental data and fitted concentration profiles for all the species present in the reaction **L2** + *cis*-[PdCl$_2$(DMF)$_2$] → **A2α-I** + **A2β-I** → **M2α-I** + **M2β**-I + *cis*-[PdCl$_2$(DMF)$_2$] → **MA2α-I** + **MA2β-I** → **D2-I**. Concentrations are given as percentages of the initial **L2** concentration. No reliable experimental data could be obtained for **MA2β-I**.

Table 2. Dynafit fitted rate constants for the cyclopalladation of ligand L2 and its monopalladated derivative M2α-I.

Rate constants	Compounds	
	L2	**M2α-I**
$k_{1\alpha}$ ($M^{-1}s^{-1}$)	0.43	–
$k_{-1\alpha}$ (s^{-1})	0.00076	
$k_{1\beta}$ ($M^{-1}s^{-1}$)	0.19	–
$k_{-1\beta}$ (s^{-1})	0.00048	
$k_{2\alpha}$ (s^{-1})	0.0019	–
$k_{2\beta}$ (s^{-1})	0.00064	–
$k_{3\alpha}$ ($M^{-1}s^{-1}$)	*	0.56
$k_{-3\alpha}$ (s^{-1})	*	0.0075
$k_{3\beta}$ ($M^{-1}s^{-1}$)	*	–
$k_{-3\beta}$ (s^{-1})	*	
$k_{4\alpha}$ (s^{-1})	0.00053	0.00054
$k_{4\beta}$ (s^{-1})	0.00048	–

*Due to significant uncertainty, these rate constants are omitted.

Kinetic modelling of NMR experiments was attempted for all reactions, but only the **L2**/**M2α-I** system produced reliable concentration profile fits for all the species in the reaction. Interestingly, this system is the one showing the largest differences between the data derived from the metalation of the **Ln** and **Mnα-I** compounds, see Table 1, indicating that it is in this reaction where the existence of a β-path is more significant. For the rest of the systems, NMR signal overlapping and poor signal-to-noise ratio did not allow the obtention of quantitative kinetic traces. Figures 7 and 8, and Table 2 collect the NMR speciation profiles, fitted kinetic traces and the

derived second order rate constants for the reaction of full cyclopalladation of **L2**, and that of its monometalated **M2α-I** intermediate, with the *cis*-[$PdCl_2(DMF)_2$].

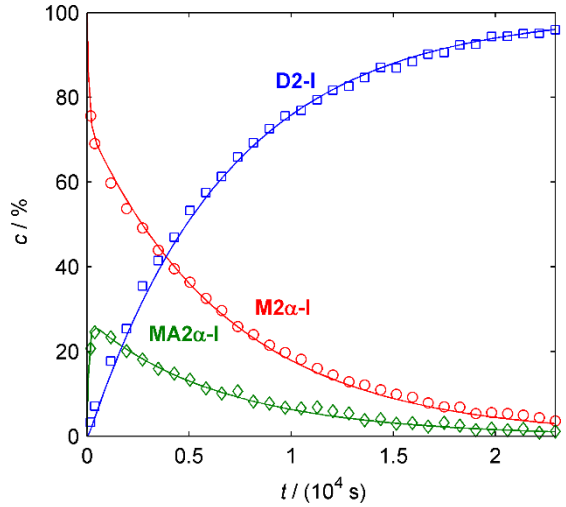

Figure 7. Experimental data and fitted concentration curves for the species present in the reaction **M2α-I** + *cis*-[$PdCl_2(DMF)_2$] → **MA2α-I** → **D2-I**. Concentrations are given as percentages of the initial **M2α-I** concentration.

For the reactions from **L1-L4** the concentration profiles indicated always higher concentrations of all α-species, compared with their β-isomers (Figures S25-S28), as expected from the preparative results indicated before. The observed difference can be interpreted as a higher stability (or a faster formation) of the α-isomers; in the case of the **Anα-I** and **Anβ-I** complexes this fact is consistent with the relation between the equilibrium constants ($K_{1\alpha}=k_{1\alpha}/k_{-1\alpha}$) > ($K_{1\beta}=k_{1\beta}/k_{-1\beta}$). Similarly, from the data collected in Table 2 we can conclude that the **M2α-I** species are formed faster than the **M2β-I** isomers, as expected for the cyclopalladation occurring preferentially on the ring bearing the electron-donating -NMe_2 group (see previous compounds section).[18]

Remarkably, the reaction of intermediate **M5-I** to produce **D5-I** was only completed after one month, under NMR concentration conditions, which effectively indicates that mono- and dipalladation processes can be considered as two fully separate processes for this system (Figures S17-S18). For the rest of the systems, the dicyclopalladated products are formed immediately once the monopalladated intermediates are present in the reaction medium (Figures S13-S16). The reaction profiles indicated that the formation rates of mono- or dipalladated species increase in the order **L5** (**M5**) < **L4** (**M4**) < **L2** (**M2**) < **L3** (**M3**) < **L1** (**M1**), which is consistent with the donor strengths of 4,4'-substituents on azobenzenes

A comparison of the results obtained from UV-Vis and NMR time-resolved experiments on the **L2** and **M2α-I** systems reveals that for the second metalation step of **L2** system, the values obtained for the second order rate constants are in extraordinary agreement (0.039 M^{-1} s^{-1} versus 0.040 M^{-1} s^{-1}), which reinforces the idea that the β path is expected to be of minor importance due to a very low K_3 value. For the first metalation step, only the order of magnitude is in agreement (0.39 M^{-1} s^{-1} versus 1.0 M^{-1} s^{-1}), a much more realistic result taking into account the large methodological differences used.

Even so, the difference for the latter can be associated very easily with the very high value of $k_{1\alpha}/k_{-1\alpha}$ obtained from the NMR measurements. This value (*ca*. 700-800 M^{-1}) should lead to the presence of an, unobserved, saturation behavior in the plots in Figures 3 and S7-S8. The difference can be associated to a very low, underestimated, value obtained for $k_{-1\alpha}$ due to limitations of the NMR technique at very short times and low concentration of the **A2α-I** species (see Figure 6).

CONCLUSIONS

We have conducted a kinetico-mechanistic study of cyclopalladation reactions involving activation of azobenzene C–H bonds by *cis*-[$PdCl_2(DMF)_2$] in DMF, both on the free ligands and on their already monopalladated derivatives. All reactions were monitored by time-resolved NMR and UV-Vis spectroscopies at different Pd-precursor concentrations, temperatures and pressures. The concentration profiles obtained by NMR monitoring enabled a direct insight into the reactivity and nature of the observed and putative intermediates, most of which have also been isolated and structurally characterized.

NMR results confirmed that the dipalladation of asymmetrically substituted azobenzenes is a multistep process involving two concurrent reaction paths. These involve an inverse sequential order for the C–H bond activation at the two possible cyclopalladation sites of the azo-derivative. A kinetic model, with a minimum number of fitting parameters, has been found capable to explain the concentration-time profiles of the reaction species. Very satisfactory results were obtained for some of the systems studied, providing a precise view of the reaction dynamics in solution. From the kinetic parameters obtained, one of the reaction paths is found to be dominant, a result also featured by the known computational study of the full process. The successful application of the kinetic model also supports the hypothesis that *bis*-palladium coordination compounds do not participate in azobenzene C–H bond activation at an appreciable extent.

Although less specific on the nature of the both reacting species and intermediates, UV-Vis monitoring has been successfully applied for the interpretation of the global kinetic model. Furthermore, the complete agreement of the data necessitates consideration of the two parallel paths resolved by NMR spectroscopy, despite one being dominant. The values of the thermal and pressure activation parameters provided additional support for the base assisted mechanism operating in these cyclopalladation reactions. These

values are consistent with a highly ordered and compressed transition state in which the basic DMF ligand participates in the proton abstraction producing an anionic species that quickly exchanges one of the two remaining chloride ligands by a new DMF ligand from the solvent. In view of the recently established distinction between the CMD mechanisms, the process evidently belongs to the *e*CMD class, as clearly indicated by the Pd-C and C-H Wiberg bond orders in the C-H activation transition states.

The results obtained represent an important contribution with a remarkable synergy between diverse but complementary techniques. This complete image of the full process will allow the better design and preparation of new cyclopalladated complexes in the Pd-catalyzed reactions of substrates having multiple C–H bonds available for functionalization.

EXPERIMENTAL SECTION

General Methods. All chemicals and solvents were of reagent grade and used without additional purifications (except the **L2** ligand). NMR spectra of MeCN-d_3, DMF-d_7, and/or DMSO-d_6 solutions were recorded on Bruker AV-600, AV-400 and, AV-300 spectrometers at 25 °C. IR spectra were recorded on an AAB Bomem MB 102 spectrophotometer using the Nujol mull method (4000-200 cm-1), and on a Perkin-Elmer Spectrum Two spectrometer. CHN analyses were carried out with a Perkin-Elmer Series II 2400 CHNS/O analyzer. PXRD data were obtained by using Ni-filtered CuK_α radiation on a PANalytical Aeris X-ray diffractometer. Single crystals structures of **A1α-I, A3α-I** and **M1α-I**, **D1-I**, were isolated from standing MeCN and DMF solutions, respectively, and were measured on an Oxford Diffraction Xcalibur Nova R (microfocus Cu tube) at 20 °C.

Kinetic Measurements. The reactions of azobenzenes and their monopalladated compounds with *cis*-[$PdCl_2(DMF)_2$] precursor were monitored by time-resolved ^{1}H NMR spectroscopy in DMF-d_7 solutions on a Bruker AV-400 spectrometer at 25 °C. Solutions for the kinetic runs were prepared by addition of 50 μL of a DMF-d_7 solution of the precursor (6.04×10^{-2} M) to 500 μL of a solution of the ligand, or the monopalladated compound, (ca. 5.5×10^{-4} M in DMF- d_7) in a NMR tube. After the addition of the *cis*-[$PdCl_2(DMF)_2$] solution, spectra were acquired at diverse time intervals, depending on the reaction rate. The kinetic traces of the species showing well resolved signals and good signal-to-noise ratio were fit with the Dynafit software.[17]

The same reactions were also followed by UV-Vis time-resolved spectroscopy at variable palladium precursor concentrations, temperatures and pressures. The variable temperature kinetic experiments at atmospheric pressure were monitored in the full 350-780 nm range on a Cary 50 UV–Vis spectrophotometer equipped with a thermostatted multicell transport (±0.1 ºC) and under pseudo-first-order conditions (palladium in at least 20-fold molar excess). The solutions were prepared by mixing the necessary volumes of a DMF solution of ligand, or monopalladated compound, with a DMF solution of *cis*-[$PdCl_2(DMF)_2$] in a 1 cm UV-Vis cuvette, the final volume was achieved by adding DMF. For the reactions carried out at varying pressure, the same sample preparation procedure was followed. The previously described pillbox cell and pressurizing system were used, and the final treatment of data was the same as described before.[4d] For these measurements, and given the excellent linearity observed for the k_{obs} versus [Pd] plots (see Figures 3 and S6-S7), the values of the second order rate constants were derived from a single k_{obs}/[Pd] ratio at a given palladium precursor concentration (as done for some other very well-behaved systems).[19] The calculation of the observed rate constants from the absorbance *versus* time monitoring of reactions was carried out using the SPECFIT software.[20] All post-run fittings were carried out using standard software. In general, the errors for the rate constants derived were within the 5 % margin.

Synthesis of Compounds. The coordination complexes (*trans*-**A1α-I**, *trans*-**A2α-I**, *trans*-**A3α-I** and **A5-III**) and monopalladated derivatives (**M1α-I**, **M2α-I**, **M3α-I**, **M4α-II**) were prepared in MeCN and DMF solution, respectively, by using the procedures recently developed for *trans*-**A2α-I** and **M2α-I**.[8] Reaction of **L4** with $PdCl_2$ in MeCN afforded the mixture of **A4α-I** and **A4α-II** structures. Monopalladated complex **M5-II** was prepared in methanol according to the previously reported procedure.[8b]

cis-[$PdCl_2(DMF)_2$] was prepared by exposing solid $PdCl_2$ (60 mg, 0.34 mmol) to DMF vapor at room temperature for 72 h. Yield: quantitative. Found: C 21.90, H 4.66, N 8.88; Calcd. for $C_6H_{14}Cl_2N_2O_2Pd$: C 22.28, H 4.36, N 8.66 (method 1). 80 mg (0.45 mmol) of $PdCl_2$ was dissolved in 10 mL of DMF and filtered off. The resulting solution was evaporated at 50 °C for 15 minutes and cooled at-25°C for two hours. The product was filtered off and dried under vacuum. Yield: 36%. (method 2).

trans-[$PdCl_2(C_6H_5N{=}NC_6H_4NMe_2)$MeCN]·MeCN, *trans*-**A1α-I** structure. A mixture of $PdCl_2$ (70 mg, 0.39 mmol) and **L1** (89 mg, 0.39 mmol) was stirred in MeCN for 30 h. The product was filtered off and dried under vacuum. Yield: 76%. Found: C 44.52, H 4.61, N 14.18; Calc. for $C_{18}H_{21}Cl_2N_5Pd$: C 44.60, H 4.37, N 14.45. ^{1}H NMR (MeCN-d_3, δ / ppm, J / Hz): 9.59 d (H-2,6, ^3J(HH)=9.4), 7.09 d (H-3,5, ^3J(HH)=9.5), 8.58 d (H-8,12, ^3J(HH)=7.5), 7.50 t (H-9,11, ^3J(HH)=7.9), 7.50 t (H-10, ^3J(HH)=7.2), 3.27 s (NMe_2).

trans-[$PdCl_2(IC_6H_4N{=}NC_6H_4NMe_2)$MeCN], *trans*-**A3α-I** structure. A mixture of $PdCl_2$ (70 mg, 0.39 mmol) and **L3** (138 mg, 0.39 mmol) was stirred in MeCN for 30 h. The product was filtered off and dried under vacuum. Yield: 88%. Found: C 33.96, H 2.88, N 10.19; Calc. for $C_{16}H_{17}Cl_2IN_4Pd$: C 33.74, H 3.01, N 9.84. ^{1}H NMR (MeCN-d_3, δ / ppm, J / Hz): 9.60 d (H-2,6, ^3J(HH)=9.3), 7.09 d (H-3,5, ^3J(HH)=9.5), 8.37 d (H-8,12, ^3J(HH)=8.5), 7.90 d (H-9,11, ^3J(HH)=8.5), 3.28 s (NMe_2).

[$PdCl_2(C_6H_4N{=}NC_6H_5)_2$], **A5-III**. A mixture of $PdCl_2$ (50 mg, 0.28 mmol) and **L5** (102 mg, 0.56 mmol) was stirred in MeCN for 30 h. The product was filtered off, washed with diethyl ether and dried under vacuum. Yield: 48%. Found: C 52.81, H 3.97, N 10.13; Calc. for $C_{24}H_{20}Cl_2N_4Pd$: C 53.21, H 3.72, N 10.34. ^{1}H NMR (DMF-d_7, δ / ppm, J / Hz): 8.43 d (H-2,6, ^3J(HH)=7.5), 7.93-7.99 m (H-3,4, 5), 8.34 d (H-8,12, ^3J(HH)=8.6), 7.67 t (H-9,11, ^3J(HH)=7.7), 7.78 t (H-10, ^3J(HH)=7.4).

[$PdCl(C_6H_5N{=}NC_6H_3NMe_2)$(DMF)], **M1α-I**. Complex *trans*-**A1α-I** (100 mg, 0.21 mmol) was stirred in DMF at room temperature for ten days. The product was filtered off and dried under vacuum. Yield 48 %. Found: C 46.86, H 4.95, N 12.55; Calc. for $C_{17}H_{21}ClN_4OPd$: C 46.48, H 4.82, N 12.76. ^{1}H NMR (DMSO-d_6, δ / ppm, J / Hz): 7.02 s, br (H-3), 6.58 d, br (H-5, ^3J(HH)= 8.4), 7.62 d (H-6, ^3J(HH)=7.6), 7.62 d (H-8, 12, ^3J(HH)=7.6), 7.35 t (H-10, ^3J(HH)=7.1), 7.42 t (H-9, 11, ^3J(HH)=7.4), 3.13 s (NMe_2).

[$PdCl(C_6H_4IN{=}NC_6H_3NMe_2)$(DMF)], **M3α-I**. Complex *trans*-**A3α-I** (100 mg, 0.18 mmol) was stirred in DMF at room temperature for seven days. The product was filtered off and dried under vacuum. Yield 67 %. Found: C 35.82, H 3.94, N 10.25; Calc. for $C_{17}H_{20}ClIN_4OPd$: C 36.13, H 3.57, N 9.91. ^{1}H NMR (DMSO-d_6, δ / ppm, J / Hz): 7.00 s, br (H-3), 6.59 d, br (H-5, ^3J(HH)= 8.6), 7.62 d, br (H-6, ^3J(HH)=8.5), 7.45 d (H-8, 12, ^3J(HH)=8.4), 7.76 d (H-9, 11, ^3J(HH)=8.6), 3.14 s (NMe_2).

[Pd(μ-Cl)($C_6H_4NO_2N{=}NC_6H_3NMe_2$)]$_2$, **M4α-II**. The mixture of complexes *trans*-**A4α-I** and **A4α-II** (100 mg) was stirred in DMF at room temperature for seven days. The product was filtered off and dried under vacuum. Yield 51 %. Found: C 40.52, H 3.44, N 13.28; Calc. for $C_{28}H_{26}Cl_2N_8O_4Pd_2$: C 40.90, H 3.19, N 13.63. ^{1}H NMR (DMSO-d_6, δ / ppm, J / Hz): 7.09 s, br (H-3), 6.69 d, br (H-5, ^3J(HH)= 8.3), 7.69 d, br (H-6, ^3J(HH)=8.5), 7.90 d (H-8, 12, ^3J(HH)=8.4), 8.26 d (H-9, 11, ^3J(HH)=8.7), 3.20 s (NMe_2).

[{PdCl(DMF)}$_2$(μ-$C_6H_4N{=}NC_6H_3NMe_2$)], **D1-I**. A mixture of **M1α-I** (100 mg, 0.23 mmol) and *trans*-[$PdCl_2(MeCN)_2$] (118 mg, 0.46 mmol) was stirred in DMF for seven days at room temperature. The product was filtered off and dried under vacuum. Yield 75%. Found: C 36.44, H 4.42, N 10.38; Calcd. for $C_{20}H_{27}Cl_2N_5O_2Pd_2$: C 36.77, H 4.17, N 10.72. ^{1}H NMR (DMSO-d_6, δ / ppm, J / Hz): 7.23 s (H-3), 6.63 d (H-5, ^3J(HH)= 9.6), 8.51 d (H-6, ^3J(HH)=9.6), 7.68 d (H-9, ^3J(HH)=7.7), 6.88 t (H-10, ^3J(HH)=7.6), 7.05 t (H-11, ^3J(HH)=7.6), 8.29 d (H-12, ^3J(HH)=8.2), 3.19 s (NMe_2).

[{PdCl(DMF)}$_2$(μ-C_6H_3ClN=$NC_6H_3NMe_2$)], **D2-I**. A mixture of **M2α-I** (100 mg, 0.21 mmol) and *trans*-[$PdCl_2(MeCN)_2$] (109 mg, 0.42 mmol) was stirred in DMF for seven days at room temperature. The product was filtered off and dried under vacuum. Yield 83%. Found: C 34.55, H 3.36, N 9.95; Calcd. for $C_{20}H_{26}Cl_3N_5O_2Pd_2$: C 34.93, H 3.81, N 10.18. ^{1}H NMR (DMSO-d_6, δ / ppm, J / Hz): 7.23 s (H-3), 6.64 d (H-5, ^3J(HH)=9.4 Hz), 8.49 d (H-6, ^3J(HH)=9.3 Hz), 7.63 s (H-9), 7.13 d (H-11, ^3J(HH)=8.7 Hz), 8.28 d (H-12, ^3J(HH)=8.7 Hz), 3.20 s (NMe_2).

[{PdCl(DMF}$_2$ (μ-C_6H_3IN=$NC_6H_3NMe_2$)], **D3-I**. A mixture of **M3α-I** (100 mg, 0.18 mmol) and *trans*-[$PdCl_2(MeCN)_2$] (91 mg, 0.35 mmol) was stirred in DMF for seven days at room temperature. The product was filtered off and dried under vacuum. Yield 73%. Found: C 31.18, H 3.01, N 9.30.; Calcd. for $C_{20}H_{26}Cl_2IN_5O_2Pd_2$: C 30.83, H 3.36, N 8.99. ^{1}H NMR (DMSO-d_6, δ / ppm, J / Hz) 7.22 s (H-3), 6.65 d (H-5, ^3J(HH)=9.8), 8.49 d (H-6, ^3J(HH)=9.4), 7.99 s (H-9), 7.44 d (H-11, ^3J(HH)=8.4), 8.04 d (H-12, ^3J(HH)=8.3), 3.19 s (NMe_2).

[{PdCl(DMF)}$_2$(μ-$C_6H_3NO_2N$=$NC_6H_3NMe_2$)], **D4-I**. A mixture of **M4α-II** (100 mg, 0.12 mmol) and *trans*-[$PdCl_2(MeCN)_2$] (123 mg, 0.48 mmol) was stirred in DMF for seven days at room temperature. The product was filtered off and dried under vacuum. Yield 75%. Found: C 34.77, H 3.41, N 11.88. Calcd. for $C_{20}H_{26}Cl_2N_6O_4Pd_2$: C 34.40, H 3.75, N 12.04. ^{1}H NMR (DMSO-d_6, δ / ppm, J / Hz): 7.30 s (H-3), 6.80 d (H-5, ^3J(HH)=9.1 Hz), 8.35 d (H-6, ^3J(HH)=9.0 Hz), 8.43 s (H-9), 7.94 d (H-11, ^3J(HH)=9.2 Hz), 8.59 d (H-12, ^3J(HH)=9.2 Hz), 3.28 s (NMe_2).

[{PdCl(DMF)}$_2$(μ-C_6H_4N=NC_6H_4)], **D5-I**. A mixture of **M5-II** (80 mg, 0.12 mmol) and *trans*-[$PdCl_2(MeCN)_2$] (128 mg, 0.49 mmol) was stirred in DMF for 14 days at room temperature. The product was filtered off and dried under vacuum. Yield 73%. Found: C 35.07, H 3.26, N 9.39.; Calcd. for $C_{18}H_{22}Cl_2N_4O_2Pd_2$: C 35.43, H 3.63, N 9.18. ^{1}H NMR (DMSO-d_6, δ / ppm, J / Hz): 7.87 d (H-3, 9, ^3J(HH)=7.2 Hz), 7.18 t (H-4, 10, ^3J(HH)=7.2 Hz), 7.14 t (H-5, 11, ^3J(HH)=7.23 Hz), 8.75 d, br (H-6, 12, ^3J(HH)=6.9 Hz).

ASSOCIATED CONTENT

Supporting Information

The Supporting Information is available free of charge on the ACS Publications website at DOI:

Additional spectra, PXRD, kinetic data and computational details including DFT geometries and their energies are given. (PDF)

Accession Codes

CCDC 1994905, 1995310-1995313 contain the supplementary crystallographic data for this paper. These data can be obtained free of charge via www.ccdc.cam.ac.uk/data_request/cif, or by emailing data_request@ccdc.cam.ac.uk, or by contacting The Cambridge Crystallographic Data Center, 12 Union Road, Cambridge CB2 1EZ, UK; fax: +44 1223 336033.

AUTHOR INFORMATION

Corresponding Author

EMAIL ADDRESSES: curic@irb.hr, dbabic@irb.hr, abudimir@pharma.hr, manel.martinez@qi.ub.edu

Notes

‡ These authors contributed equally. The authors declare no competing financial interests.

ACKNOWLEDGMENT

This work has been supported by Croatian Science Foundation under project number IP-2019-04-9951 and by the Spanish Ministerio de Ciencia e Innovación under project PID2019-107006GB-C21. Computations were done on the Isabella cluster at SRCE, Zagreb.

REFERENCES

1) (a) Whitehurst, W. G.; Gaunt, M. J. Synthesis and Reactivity of Stable Alkyl-Pd(IV) Complexes Relevant to Monodentate N-Directed C(sp^3)−H Functionalization Processes. *J. Am. Soc.* **2020**, *142*, 14169–14177. https://doi.org/10.1021/jacs.0c04732. (b) Dickmu, D. C.; Smoliakova, I. P. Cyclopalladated complexes containing an (sp(3))C-Pd bond. *Coord. Chem. Rev.* **2020**, *409*, 21320. https://doi.org/10.1016/j.ccr.2020.213203. (c) Tylkowski, B.; Trojanowska, A.; Marturano, V.; Nowak, M.; Marciniak, L.; Giamberini, M.; Ambrogi, V.; Cerruti, P. Power of light-Functional complexes based on azobenzene molecules. *Coord. Chem. Rev.* **2017**, *351*, 205-217. https://doi.org/10.1016/j.ccr.2017.05.009. (d) Kapdi, A. R.; Fairlamb, I.J. S. Anti-cancer palladium complexes: a focus on PdX_2L_2, palladacycles and related complexes. *Chem. Soc. Rev.* **2014**, *43*, 4751-4777. https://doi.org//10.1039/c4cs00063c. (e) Dehand, J.; Pffefer,M. Cyclometallated Compounds. *Coord. Chem. Rev.* **1976**, *18*, 327-352. http://dx.doi.org/10.1016/S0010-8545(00)80431-2. (f) Omae, I. Intramolecular five-membered ring compounds and their applications. *Coord. Chem. Rev.* **2004**, *248*, 995-1023. https://doi.org/10.1016/j.ccr.2004.05.011. (g) Albrecht, M. Cyclometalation Using d-Block Transition Metals: Fundamental Aspects and Recent Trends. *Chem. Rev.* **2010**, *110*, 576-623. https://doi.org/10.1021/cr900279a. (h) Dupont, J.; Consorti, C. S.; Spencer, J. The Potential of Palladacycles: More than Just Precatalysts. *Chem. Rev.* **2005**, *105*, 2527-2572. https://doi.org/10.1021/cr030681r. (i) *Palladacycles: Synthesis, Characterization and Applications* (Eds. Dupont, J.; Pfeffer, M.), Wiley-VCH, Weinheim, **2008**. (j) Ghedini, M.; Aiello, I.; Crispini, A.; Golemme, A.; La Deda, M.; Pucci, D. Azobenzenes and Heteroaromatic Nitrogen Cyclopalladated Complexes for Advanced Applications. *Coord. Chem. Rev.* **2006**, *290*, 1373-1390. https://doi.org/10.1016/j.ccr.2005.12.011. (k) Wakatsuki, Y.; Yamazaki, H.; Grutsch, P. A.; Santhanam, M.; Kutal, C. Study of Intramolecular Sensitization and Other Excited-State Pathways in Orthometalated Azobenzene Complexes of Palladium(II). *J. Am. Chem. Soc.* **1985**, *107*, 8153-8159. https://doi.org/10.1021/om9609574.

(2) (a) Chen, Y.-Q.; Singh, S.; Wu, Y. Wang, Z.; Hao, W.; Verma, P.; Qiao, J. X.; Sunoj, R. B. Yu, J.-Q. Pd-Catalyzed γ-C(sp^3)−H Fluorination of Free Amines. *J. Am. Chem. Soc.* **2020**, *142*, 9966−9974. https://dx.doi.org/10.1021/jacs.9b13537. (b) Park, H. S.; Fan, Z.;Zhu, R.-Y.; Yu, J.-Q. Distal γ -C(sp^3)−H Olefination of Ketone Derivatives and Free Carboxylic Acids *Angew. Chem. Int, Ed*. **2020**, *132*, 12953–12959. https://doi.org/10.1002/anie.202003271. (c) Wang, L.; Carrow, B. P. Oligothiophene Synthesis by a General C−H Activation Mechanism: Electrophilic Concerted Metalation-Deprotonation (eCMD). *ACS Catal*. **2019**, *9*, 6821–6836. https://doi.org/10.1021/acscatal.9b01195. (d) Qian, S.; Li, Z.-Q.; Li, M.; Wisniewski, S. R.; Qiao, J. X.; Richter, J. M.; Ewing, W. R.; Eastgate, M. D.; Chen, J. S.; Yu, J.-Q. Ligand-Enabled Pd(II)-Catalyzed C(sp^3)–H Lactonization Using Molecular Oxygen as Oxidant. *Org. Lett*. **2020**, *22*, 3960−3963. https://dx.doi.org/10.1021/acs.orglett.0c01243. (e) Malapit, C. A.; Ichiishi, N.; Sanford, M. S. Pd-Catalyzed Decarbonylative Cross-Couplings of Aroyl Chlorides. *Org. Lett*. **2017**, *19*, 4142−4145. https://dx.doi.org/10.1021/acs.orglett.7b02024. (f) Topczewski, J. J.; Cabrera, P. J.; Saper, N. I.; Sanford, M. S. Palladium-Catalyzed Transannular C–H Functionalization of Alicyclic Amines. *Nature*, **2016**, *531*, 220-224. https://dx.doi.org/10.1038/nature16957. (g) Ryabov, A. D. Cyclopalladated

Complexes in Organic Synthesis. *Synthesis* **1985**, 233-252. https://doi.org/10.1055/s-1985-31169 3. (h) McNally, A.; Haffemayer, B.; Collins, B. S. L.; Gaunt, M. J. Palladium-Catalysed C–H Activation of Aliphatic Amines to Give Strained Nitrogen Heterocycles. *Nature*, **2014**, *510*, 129-133. https://doi.org/10.1038/nature13389. (i) Yamaguchi, J.; Yamaguchi, A. D.; Itami, K. C–H Bond Functionalization: Emerging Synthetic Tools for Natural Products and Pharmaceuticals. *Angew. Chem. Int. Ed*. **2012**, *51*, 8960-9009.
https://doi.org/10.1002/anie.201201666. (j) Ackermann, L. Carboxylate-Assisted Transition-Metal-Catalyzed C-H Bond Functionalizations: Mechanism and Scope. *Chem. Rev*. **2011**, *111*, 1315-1345. https://doi.org/10.1021/cr100412j. (k) Godula, K.; Sames, D. C-H Bond Functionalization in Complex Organic Synthesis. *Science*, **2006**, *312*, 67-62. https://doi.org/10.1126/science.1114731. (l) Lyons, T; W. Sanford, M. S. Palladium-Catalyzed Ligand-Directed C−H Functionalization Reactions. *Chem, Rev*. **2010**, *110*, 1147-1169.
https://doi.org/10.1021/cr900184e.

(3) (a) Granell, J.; Martinez M. Kinetico-mechanistic studies of cyclometalating C–H bond activation reactions on Pd(II) and Rh(II) centres: The importance of non-innocent acidic solvents in the process. *Dalton Trans.* **2012**, *41*, 11243-11258.
https://doi.org/10.1039/c2dt30866e. (b) Laga, E.; Garcia-Montero, A.; Sayago, F. J.; Soler, T.; Moncho, C.; Cativiela, C.; Martinez, M.; Urriolabeitia, E. P. Cyclopalladation and Reactivity of Amino Esters through C–H Bond Activation: Experimental, Kinetic, and Density Functional Theory Mechanistic Studies. *Chem. Eur. J*. **2013**, *19*, 17398-17412. https://doi.org/10.1002/chem.201302693. (c) Roiban, G.D.; Serrano, E.; Soler, T.; Aullón, G.; Grosu, I.; Cativiela, C.; Martinez, M.; Urriolabeitia, E. P. Regioselective Orthopalladation of (Z)-2-Aryl-4-Arylidene-5(4H)-Oxazolones: Scope, Kinetico-Mechanistic, and Density Functional Theory Studies of the C–H Bond Activation. *Inorg. Chem*. **2011**, *50*, 8132-8143. https://doi.org/10.1021/ic200564d. (d) Ryabov, A. D.; Sakodinskaya, I. K.; Yatsimirski, A. Kinetics and Mechanism of *Ortho*-Palladation of Ring-Substituted *N,N*-dimethylbenzylAmines K. *J. Chem. Soc. Dalton Trans*. **1985**, 2629-2638.
https://doi.org/10.1039/DT9850002629. (e) Yagyu, T.; Aizawa, S.; Funahashi, S. Mechanistic Studies on Cyclopalladation of the Solvated Palladium(II) Complexes with *N*-Benzyl Triamine Ligands in Various Solvents. Crystal Structures of $[Pd(Sol)(Bn_2Medptn)](BF_4)_2$ (Sol = Acetonitrile and *N,N*-Dimethylformamide; $Bn_2Medptn$ = *N,N′*-Dibenzyl-4-methyl-4-azaheptane-1,7-diamine) and $[Pd(H_{-1}Bn_2Medptn\text{-}C,N,N',N'')]CF_3SO_3$. *Bull. Chem. Soc. Jpn*. **1998**, *71*, 619-629. https://doi.org/10.1246/bcsj.71.619. (f) Yagyu, T.; Iwatsuki, S.; Aizawa, S.; Funahashi, S. Electronic Effect of Substituents on Cyclopalladation of the Solvated Palladium(II) Complexes with *N*-Benzyl Triamine $[Pd(Sol)\{(4\text{-}XC_6H_4CH_2)NH(CH_2)_3NR(CH_2)_3NH_2\}]^{2+}$(Sol = Solvent; R = Ph, H, and Me; X = H, Et, Me, MeO, Cl, and NO_2). *Bull. Chem. Soc. Jpn*. **1998**, *71*, 1857-1862. https://doi.org/10.1246/bcsj.71.1857. (g) Gomez, M.; Granell, J.; Martinez, M. Mechanisms of Cyclopalladation Reactions in Acetic Acid: Not So Simple One-Pot Processes. *Eur. J. Inorg. Chem*. **2000**, 217-224. https://doi.org/10.1002/(SICI)1099-0682(200001)2000:1<217::AID-EJIC217>3.0.CO;2-Q.

(4) (a) Babić, D.; Ćurić, M.; Smith, D. M. Computational Study of the Cyclopalladation Mechanism of Azobenzene with $PdCl_2$ in *N,N*-Dimethylformamide. *J. Organomet. Chem*. **2011**, *696*, 661-669. https://doi.org/10.1016/j.jorganchem.2010.09.038. (b) Juribašić, M.; Budimir, A.; Kazazić, S.; Ćurić, M. Dicyclopalladated Complexes of Asymmetrically Substituted Azobenzenes: Synthesis, Kinetics and Mechanisms. *Inorg. Chem*. **2013**, *52*, 12749-12757.
https://pubs.acs.org/doi/10.1021/ic402017v. (c) Aullón, G.; Chat, R.; Favier, I.; Font-Bardia, M.; Gomez, M.; Granell, J.; Martinez, M.; Solans, X. Cyclometallation of amino-imines on palladium complexes. The effect of the solvent on the experimental and calculated mechanism. *Dalton Trans*, **2009**, 8292-8300. https://doi.org/10.1039/B905134A.
(d) Font, H.; Font-Bardia, M.; Gómez, K.; González, G.; Granell, J.; Macho, I.; Martínez, M. A kinetico-mechanistic study on the C–H bond activation of primary benzylamines; cooperative and solid-state cyclopalladation on dimeric complexes. *Dalton Trans.* **2014**, 13525–135236.
https://doi.org/10.1039/C4DT01463D. (e) Gomez, M.; Granell, J.; Martinez, M. Variable-temperature and-pressure kinetics and mechanism of the cyclopalladation reaction of imines in aprotic solvent. *Organometallics*, **1997**, *16*, 2593-2546.
https://doi.org/10.1021/om961099e. (f) Favier, I.; Gomez, M.; Granell, J.; Martinez., M.; Font-Bardia, M.; Solans, X.; Font-Bardia, M. Kinetico–mechanistic studies of C–H bond activation on new Pd complexes containing *N,N′*-chelating ligands. *Dalton. Trans.* **2005**, 123-132. https://doi.org/10.1039/B415613G.

(5) (a) Grimster, N. P.; Gauntlett, C.; Godfrey, C. R. A.; Gaunt, M. J. Palladium-Catalyzed Intermolecular Alkenylation of Indoles by Solvent-Controlled Regioselective C−H Functionalization. *Angew. Chem., Int. Ed*. **2005**, *44*, 3125-3129. https://doi.org/10.1002/anie.200500468. (b) Ulery, H. E. A Novel Preparation of Amidinium Arsenesulfonates. *J. Org. Chem*. **1965**, *30*, 2464-2465. https://doi.org/10.1021/jo01018a510. (c) Mei, T. S.; Wang, X.; Yu, J.-Q. Pd(II)-Catalyzed Amination of C−H Bonds Using Single-Electron or Two-electron Oxidants. *J. Am. Chem. Soc*. **2009**, *131*, 10806-10807. https://doi.org/10.1021/ja904709b. (d) Chiong, H. A.; Pham, Q. N.; Daugulis, O. Two Methods for Direct ortho-Arylation of Benzoic Acids. *J. Am. Chem. Soc.* **2007**, *129*, 9879-9884.
https://doi.org/10.1021/ja071845e. (e) Zaitsev, V. G.; Daugulis, O. Highly Regioselective Arylation of sp^3 C−H Bonds Catalyzed by Palladium Acetate. *J. Am. Chem. Soc.* **2005**, *127*, 13154-13155.
https://doi.org/10.1021/ja054549f.

(6) (a) Mottillo, C.; Lu, Y.; Pham, M.-H.; Cliffe, M. J.; Do, T.-O.; Friščić, T. Mineral Neogenesis as an Inspiration for Mild, Solvent-Free Synthesis of Bulk Microporous Metal–Organic Frameworks from Metal (Zn, Co) Oxides. *Green Chem*. **2013**, *15*, 2121.
https://doi.org/10.1039/C3GC40520F. (b) Cliffe, M. J.; Mottillo, C.; Bučar, D.-K.; Friščić, T. Accelerated Aging: a Low Energy, Solvent-Free Alternative to Solvothermal and Mechanochemical Synthesis of Metal–Organic Materials *Chem. Sci*. **2012**, *3*, 2495.
https://doi.org/10.1039/C2SC20344H (c) Braga, D.; Giaffreda, S. L.; Grepioni, F.; Chierotti, M. R.; Gobetto, R.; Palladino, G.; Polito, M. Solvent Effect in a “Solvent Free” Reaction. *CrystEngComm.* **2007**, *9*, 879.
https://doi.org/10.1039/B711983F (d) Monas, A.; Užarević, K.; Halasz, I.; Juribašić Kulcsár, M.; Ćurić, M. Vapour-Induced Solid-State C–H bond Activation for the Clean Synthesis of an Organopalladium Biothiol Sensor. *Chem. Commun.* **2016**, *52*, 12960-12963.
https://doi.org/10.1039/C6CC06062E.

(7) (a) Donati, M.; Morelli, D.; Conti, F.; Ugo, R. Complessi dimetilammidici di alcuni metalli del grupo del platino, *Chim. Ind.* **1968**, 50, 231-235. (b) Wayland, B. B.; Schramm, R. F. Cationic and Neutral Chloride Complexes of Palladium(II) with the Nonaqueous Solvent Donors Acetonitrile, Dimethyl Sulfoxide, and a Series of Amides. Mixed Sulfur and Oxygen Coordination Sites in a Dimethyl Sulfoxide Complex, *Inorg. Chem.* **1969**, 8, 971-976. https://doi.org/10.1021/ic50074a050. (c) Gioria, J. M.; Susz, B. P. Etude des composés d'addition des acides de Lewis – XXXV. Note sur les composés d'addition entre amides et, respectivement, $PdCl_2$ et $PtCl_2$, *Helv. Chim. Acta* **1971**, 54, 2251-2256. https://doi.org/10.1002/hlca.19710540762.

(8) Bjelopetrović, A.; Lukin, S.; Halasz, I.; Užarević, K.; Đilović, I.; Barišić, D.; Budimir, A.; Juribašić Kulcsár, Ćurić, M. Mechanism of Mechanochemical C-H Bond Activation in an Azobenzene Substrate by Pd(II) Catalysts. *Chem. Eur. J.* **2018**, *24*, 10672.
https://doi.org/10.1002/chem.201802403.

(9) Juribašić Kulcsár, M.; Halasz, I.; Babić, D.; Cinčić, D.; Plavec, J.; Ćurić, M. Aging and Ball-Milling as Low-Energy and Environmentally Friendly Methods for the Synthesis of Pd(II) Photosensitizers. *Organometallics*, **2014**, *33*, 1227-1234.
https://doi.org/10.1021/om500008v.

(10) Khare, G. P.; Little, R. G.; Veal, J. T.; Doedens, R. J. Crystal and Molecular Structure of Dichlorobis(azobenzene)palladium(II), a Possible Intermediate in the Ortho Palladation of Azobenzene. *Inorg. Chem*. **1975**, *14*, 2475-2479. https://doi.org/10.1021/ic50152a037.

(11) Ćurić, M.; Tušek-Božić, Lj.; Vikić-Topić, D.; Scarcia, V.; Furlani, A.; Balzarini, J.; DeClercq, E. Palladium(II) Complexes of Dialkyl α-Anilinobenzylphosphonates. Synthesis, Characterization, and Cytostatic activity. *J. Inorg. Biochem*. **1996**, *63*, 125-142. https://doi.org/10.1016/0162-0134(95)00199-9.

(12) Roy, S.; Hartenbach, I.; Sarkar, B. Structures, Redox and Spectroscopic Properties of Pd^{II} and Pt^{II} Complexes Containing an Azo Functionality. *Eur. J. Inorg. Chem.* **2009**, 2553–2558. https://doi.org/10.1002/ejic.200900007.

(13) (a) Babić, D.; Ćurić, M.; Molčanov, K.; Ilc, G.; Plavec, J. Synthesis and Characterization of Dicyclopalladated Complexes of Azobenzene Derivatives by Experimental and Computational Methods. *Inorg. Chem.* **2008**, *47*, 10446-10454. https://doi.org/10.1021/ic8010234. (b) Ćurić, M.; Babić, D.; Višnjevac, A; Molčanov, K. Simple Route to the Doubly ortho-Palladated Azobenzenes: Building Blocks for Organometallic Polymers and Metallomesogens. *Inorg. Chem*. **2005**, *44*, 5975. https://doi.org/10.1021/ic050747w.

(14) Ryabov, A. D. Mechanisms of intramolecular activation of carbon-hydrogen bonds in transition-metal complexes. *Chem. Rev*. **1990**, *90*, 403-424. https://doi.org/10.1021/cr00100a004.

(15) (a) Espenson, J. H. Chemical Kinetics and Reaction Mechanisms, McGraw-Hill, New York, **1981**. (b) Tobe, M. L.; Burgess, J. Inorganic Reaction Mechanisms, Longman, New York, **1999**.

(16) (a) Carrow, B. P.; Sampson, J.; Wang, L. Base-Assisted C−H Bond Cleavage in Cross-Coupling: Recent Insights into Mechanism, Speciation, and Cooperativity. *Isr. J. Chem*. **2019**, 59, 230–258. https://doi.org/10.1002/ijch.201900095. (b) Alharis, R. A.; McMullin, C. L. Davies, D. L.; Singh, K.; Macgregor, S. A. The Importance of Kinetic and Thermodynamic Control when Assessing Mechanisms of Carboxylate-Assisted C−H Activation. *J. Am. Chem. Soc*. **2019**, *141*, 8896−8906. https://doi.org/10.1021/jacs.9b02073. (c) Yang, Y.-F.; Yu, J.-Q.; Houk, K. N. Experimental-Computational Synergy for Selective Pd(II)-Catalyzed C–H Activations of Aryl and Alkyl Groups. *Acc. Chem. Res*. **2017**, *50*, 2853-2860. https://doi.org/10.1021/acs.accounts.7b00440. (d) Yang, Y.-F.; Cheng, G.-J.; Liu, P.; Leow, D.; Sun, T.-Y.; Chen, P.; Zhang, P.; Yu, J.-Q.; Wu, Y.-D.; Houk, K, N. Palladium-Catalyzed Meta-Selective C−H Bond Activation with a Nitrile-Containing Template: Computational Study on Mechanism and Origins of Selectivity. *J. Am. Chem. Soc*. **2014**, *136*, 344−355. https://doi.org/10.1021/ja410485g.(e) Jiang, J.; Yu, J.-Q.; Morokuma, KMechanism and Stereoselectivity of Directed C(sp^3)−H Activation and Arylation Catalyzed by Pd(II) with Pyridine Ligand and Trifluoroacetate: A Computational Study. *ACS Catal*. **2015**, *5*, 3648−3661. https://doi.org/10.1021/cs501626n. (f) Davies, D. L.; Macgregor, S. A.; McMullin, S. A. Computational Studies of Carboxylate-Assisted C−H Activation and Functionalization at Group 8−10 Transition Metal Centers. *Chem. Rev*. **2017**, *117*, 8649−8709. https://doi.org/10.1021/acs.chemrev.6b00839. (g) Wang, P.; Verma, P.; Xia, G.; Shi, J.; Qiao, J. X.; Tao, S.; Cheng, P. T. W.; Poss, M. A.; Farmer, M. E.; Yeung, K.-S.; Yu, J.-Q. Ligand-accelerated non-directed C–H functionalization of arenes. *Nature*, **2017**, *551*, 489-493. https://doi.org/10.1038/nature24632. (h) Engle. K. M.; Wang, D.-H.; Yu, J.-Q. Ligand-Accelerated C-H Activation Reactions: Evidence for a Switch of Mechanism. *J. Am. Chem. Soc*. **2010**, *132*, 14137–14151. https://doi.org/10.1021/ja105044s.

(17) (a) Kuzmič, P. Program DYNAFIT for the analysis of enzyme kinetic data: Application to HIV proteinase. *Anal. Biochem*. **1996,** *237*, 269-273. https://doi.org/10.1006/abio.1996.0238. (b) Kuzmič, P. DYNAFIT – a software package for enzymology. Methods Enzymol. **2009,** *467*, 247-280. https://doi.org/10.1016/S0076-6879(09)67010-5.

(18) Wakatsuki, Y.; Yamazaki, H.; Grutsch, P. A.; Santhanam, M.; Kutal, C. Study of intramolecular sensitization and other excited-state pathways in orthometalated azobenzene complexes of palladium(II). *J. Am. Chem. Soc.* **1985**, *107*, 8153-8159. https://doi.org/10.1021/om9609574.

(19) Bernhard, P. V.; Gonzálvez, M.V.; Martinez, M. Kinetico-mechanistic Study on the Oxidation of Biologically Active Iron(II) Bis(thiosemicarbazone) Complexes by Air. Importance of NH···O_2 Interactions as Established by Activation Volumes. *Inorg. Chem*. **2017**, *56*, 1428-14290. https://pubs.acs.org/doi/abs/10.1021/acs.inorgchem.7b02381.

(20) Binstead, R. A.; Züberbuhler A. D.; Jung, B. SPECFIT32. [3.0.34], Spectrum Software Associates, **2005**.

Table of Contents Synopsis

A kinetico-mechanistic study of the C–H bond activation in azobenzenes and their monopalladated derivatives with *cis*-[$PdCl_2(DMF)_2$] in DMF has been conducted by time-resolved NMR and UV-Vis spectroscopies at variable concentration, temperature and pressure. NMR spectra enabled detailed insight into the nature and reactivity of intermediates and confirmed that the dipalladation of 4,4′-functionalized azobenzenes is a multistep process involving two reaction pathways.